IEEE Access
Multidisciplinary | Rapid Review | Open Access Journal

Received September 5, 2018, accepted September 19, 2018, date of publication September 24, 2018,
date of current version October 17, 2018.

Digital Object Identifier 10.1109/ACCESS.2018.2871776

Multi-Island Genetic Algorithm and Kriging Model-Based Design of Vehicle Product Comprising Multi-Material

FANGWU MA[1], LU HAN[1], YANG ZHOU[2], SHIXIAN CHEN[1], AND YONGFENG PU[1]
[1]State Key Laboratory of Automotive Simulation and Control, Jilin University, Changchun 130022, China
[2]FAW Vehicle Development Department, Changchun 130025, China

Corresponding authors: Lu Han (hanlu.jay@163.com) and Yongfeng Pu (puyongfeng@jlu.edu.cn)

This work was supported in part by the National Key Research and Development Program of China under Grant 2016YFB0101601, and in part by the Special Project of Jilin Province and Jilin University under Grant SXGJQY2017-7 and Grant SXGJQY2017-2-1-5.

ABSTRACT In recent years, improvement in multi-material additive manufacturing technology has resulted in technical improvements in multi-material design employed by the automotive industry. Therefore, in this work, an internal trim part (corresponding to an original product composed of polypropylene) of a vehicle was divided into four components using a multi-material design method considering PLA composites. The PLA was reinforced with basalt fibers for realization of the required mechanical properties. The mechanical properties associated with different fiber content (from 0 to 60%) were determined via tensile tests. To reduce the mass of the product, an optimization process combining a Kriging surrogate model with a Multi-Island Genetic Algorithm was used to search for the Pareto solution. The coefficient of determination (R^2) and response surface methodology (RSM) surrogate model were used to confirm the validity and accuracy of the Kriging model. The values of R^2 were all >0.92 and the low error value of both results demonstrated the effectiveness of the optimization process. Owing to the optimization process, the mass of the PLA composite product was reduced by nearly 9%. Correlation analysis indicated that x_2 has the strongest impact on the total mass. Therefore, the optimization process proposed for the multi-material optimal design is feasible and contributes significantly to the attainment of light-weight vehicle parts.

INDEX TERMS Automotive components, biodegradable materials, materials testing, genetic algorithms, mathematical model.

I. INTRODUCTION

Poly lactic acid (PLA) is the most extensively researched and one of the best environmentally friendly substitutes for non-renewable polymers [1]–[3]. Original equipment manufacturers (OEMs) have used PLA, as alternatives for fossil materials, in the production of internal and external automotive body parts of vehicles, owing to the environmental friendliness of these materials, because intelligence and ecology are the trend of automobile industry [4]–[11]. The use of PLA composites yields a reduction in petroleum consumption and is, hence, beneficial to companies, the environment, and end-customers [12]. Although Ford Fiesta manufacturers have played a pioneering role in adopting biopolymers and biocomposite, few parts are fabricated from renewable materials [4], [13]–[15]. Fiber reinforcement is typically employed to overcome the main obstacles that prevent wide-range application of these materials. Basalt fibers exhibit excellent mechanical properties and stability compared with glass fibers and are therefore considered one of the most suitable natural fibers [16]–[19]. However, studies considering PLA reinforced by basalt fibers have rarely been reported.

Multi-material design contributes significantly to reductions in the vehicle mass, especially with the development of additive manufacturing processes for automotive constructions. These processes can generate complex multi-material parts (rather than the traditional single-material parts) [20]–[24]. Multi-material design, which is considered essential for sustainability of the automotive industry [25], contributes to the realization of product efficiency and multi-material systems exhibiting good performance [26]. This indicates that the hardness, corrosion resistance, and environmental adaptability of a single component can be defined under the most stringent conditions [27]. Excellent properties have been achieved for PLA composites

used as raw material for additive manufacturing processes, such as three-dimensional (3D) printing [28], [29]. Therefore, in this study, for improved material-function compatibility and product efficiency of the overall product, an injection-molded product is divided into several components composed of different materials.

Multi-material design used in product design has become a complex multi-disciplinary and multi-stage design process [30]. Many solutions satisfy the requirements and, hence, an efficient optimization method is essential. Ideal solutions can be identified by employing optimization methods, e.g., a Genetic Algorithm (GA). This method is characterized by a simple currency and strong robustness and has therefore attracted significant attention in recent years [15], [31]–[34]. However, shortcomings including a poor local search, premature convergence, and slow convergence rate have limited the application of GA. Improvements to this method are therefore required [31]. Multi-Island Genetic Algorithm (MIGA) is considered an efficient and reliable algorithm for treating non-linear and multi-disciplinary problems associated with the optimization methods [35]–[39]. As in the case of GA, MIGA is based on the natural evolution course of several islands. The definition of MIGA is simple and can be easily enacted. Furthermore, MIGA can avoid the local optimal solution set and is more effective than the traditional GA [32]. The surrogate modeling of responses has become a common method of reducing the computation time required for the repeated evaluation of responses [40]. By using simultaneous approximations, the constraints and objectives from different types of analyses can be optimized in the same loop [38], [41]. The Kriging model can accurately pass through all the sample points lying in the design space. This model is based on deterministic simulations where the same inputs always yield the same output, without noise [38], [42]. The effectiveness and accuracy of MIGA combined with a Kriging model have been demonstrated in several studies. Paz *et al.* [43] used GA and a Kriging model to realize the design of light-weight parameters in four-dimensional (4D) printing parts. Yang *et al.* [44] employed this combination to simulate the riding quality index and optimize the parameters of the suspension. The riding quality improved significantly, indicating the universality and effectiveness of this approach. Similarly, Lee *et al.* optimized multiple wing sails using MIGA combined with a Kriging model. Li *et al.* [45] have shown that, compared with GAs, a Kriging metamodel-assisted MIGA converges more rapidly to the Pareto frontier. Owing to the aforementioned advantages, in this work, a Kriging model combined with MIGA is employed as the optimization process for determining the Pareto solution.

In this work, PLA composites with different content of basalt fibers are fabricated and the corresponding mechanical properties are determined through standard tensile tests. Actual operation conditions, to be used as constraints for the objective function, are formulated by collecting the loading spectra of the product in a real vehicle subjected to full and half load. For high product efficiency, the one part is divided into four components with different kind of PLA composites. Optimal Latin hypercube experiment design is used to construct the sample points for building a Kriging model, which is then compared with RSM model [46]. The accuracy of each model is evaluated in terms of R^2 values. Using the minimum mass as an objective function with constraints, the problem is solved using a Multi-Island Genetic Algorithm (MIGA). In addition, a correlation coefficient is used to express the effect of variables on the objective function. This optimization process yields materials with improved properties. Compared with previous studies, this study makes three contributions: 1) Improved PLA material reinforcing with different content of short basalt fibers is potential renewable materials for Eco-Car design that is an important developing direction. The data of PLA composites in this work is suitable for future eco-designs in automotive. 2) In this work, the method of manufacturing a component with several kinds of material instead of one material is used basing on the development of additive manufacturing processes for realization of light-weight products. 3) The results demonstrate the optimization process combining MIGA and the Kriging model is effective for multi-material optimal design aimed at achieving light-weight products.

II. MECHANICAL PROPERTIES

Injection molding-grade PLA, type 290 D made in Taizhou, Zhejiang province, is supplied by Zhejiang Hisun Biomaterials Co. Ltd. The properties characterizing this type of PLA are summarized as follows: density: 1.25 g/cm^3, glass transition temperature: ∼58 °C, and melting temperature: 175–180 °C. The *Mn* and *Mw*/*Mn* values are 6.5 × 10^4 g/mol and 1.38, respectively. Chopped basalt fibers (initial fiber length: 6 mm; average fiber diameter: 13 μm) are purchased from Jilin Tong Xin Basalt Technology Co. Ltd. A silane treatment for asphalt paint is applied to the fibers.

Prior to fabrication of the composite, PLA pellets are dried in a vacuum oven at 70 °C for at least 48 h. Although hydrolysis of basalt fibers is difficult, the fibers are dried in the oven for 24 h at 110 °C to remove residual moisture from their surface. PLA-based composites with a nominal basalt fiber content of 10, 20, 30, 40, 50, and 60 wt.% are prepared using a torque rheometer (XSS-300, Shanghai; working capacity: 50 g). The basalt fiber-reinforced PLA samples and pure PLA samples are injection-molded (injection pressure: 450 bar, holding pressure: 150 bar, holding time: 17 s) using a Thermo Scientific HAAKE Mini Jet Pro injection molding machine. The melt and mold temperatures are set to 205 °C and 25 °C, respectively.

The properties of the composites are determined via tensile tests, performed in accordance with the ISO 527-2 standard. The tests were conducted at 23 ± 2 °C and 50 ± 5% relative humidity (RH) on a WSM-20kN electronic universal testing machine (Changchun Intelligent Instrument Equipment Co., Ltd.; max force: 20 kN, testing precision: ±0.1%). Based on ISO 527-2, dumbbell-type 5A samples (total length: 75 mm,

length of 2 × 4 mm cross-section: 25 mm) are tested (loading speed: 1 mm/min). At least five specimens of each composite type are tested. In addition, the tensile strength and tensile modulus are computed from the stress-strain curves.

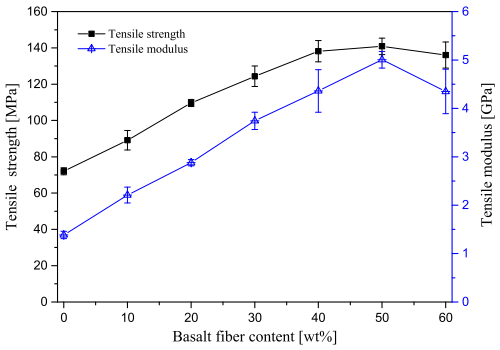

FIGURE 1. Tensile property results.

The mechanical properties of the injection-molded specimens are analysed via quasi-static tensile tests. Figure 1 indicates that improved tensile properties can be realized by using basalt fiber-reinforced PLA composites with high fiber content. The tensile strength and tensile modulus of pure PLA are 72 MPa and 1360 MPa, respectively. The strength and modulus increase with increasing basalt fiber content. In fact, for a fiber content of 50%, the strength increases (by a factor of 1.94) to a maximum of 140 MPa and the modulus increases (by a factor of 2.7) to 5050 MPa. This indicates that basalt can yield improved tensile properties of the PLA composites. However, the tensile strength of the composite with 60% basalt (i.e., 136 MPa) is lower than that (140 MPa) of the composite with 50% basalt. The same trend is observed for the tensile modulus; the tensile modulus of the composite with 60% basalt (i.e., 4350 MPa) is significantly lower than that (5050 MPa) of the composite with 50% basalt. The properties of the PLA composites are shown in Table 1.

III. LOAD ANALYSIS AND NUMERICAL RESULTS

For replacement of the petroleum-based material in automotive products, internal trim parts, which serve in a more temperate environment than the external ones, are considered suitable for fabrication from PLA composites. An internal trim part composed of PP and located before the AT change lever is investigated in this work. Knowledge of the actual load is essential for the analysis and design of PLA-composite parts. The part is fixed in the auxiliary console using six screws (as shown in Figure 3).

The durability and structural strength of this part are assessed via reliability testing of the vehicle. Full load and half load tests are performed, where the load is measured by an acceleration sensor located in the middle of the part. The sampling frequency is set to 500 Hz. The modal frequency is analyzed via FFT (see Figure 3 for the load spectrum). As the figure shows, during testing, the product is subjected to loading in three directions. In the half-load process, the Y-direction load, i.e., the maximum load, reaches

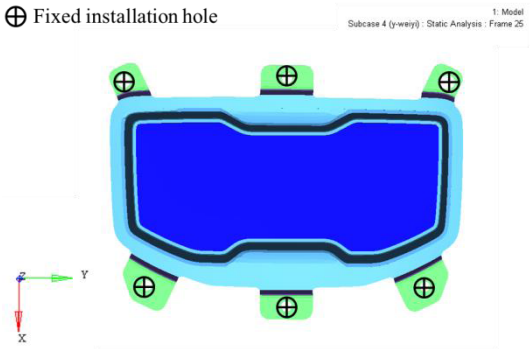

FIGURE 2. Configuration of work conditions.

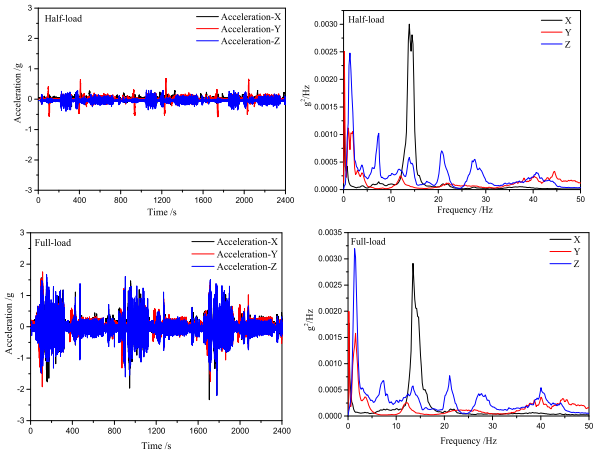

FIGURE 3. Load spectra of full load and half load.

0.86 g (g: gravitational acceleration). The Z-direction load reaches 2.33 g in full load. The maximum of the two loads, through the radial four valve chamber (RFVC), is 1.39 g and 2.41 g, respectively. Moreover, based on the mass of the part, the force on the part is 4.39 N. The part can resist deformation from three directions. However, the force considered in the quasi-static finite element analysis is lower than that required to induce deformation. The stiffness of the part is included in the boundary conditions associated with the design of the new product, by using a 100-N force to replace the actual load from each of the three directions. The maximum displacement under the three-direction force is used to represent the stiffness of the part (see Figure 4 for the details of the force). Quasi-static finite element analysis with the 100-N force is performed independently.

The modal of a part plays the key role in avoiding the main resonance frequency of a vehicle. The FFT result shows this frequency. Two types of loads yield similar main resonance frequency in three directions. The maximal resonance frequency in the X, Y, and Z directions is 14 Hz, 2 Hz, and 2 Hz, respectively. Furthermore, the modal of the original product is determined via numerical simulation.

A shell finite element model is first constructed in Hyperwork software to analyze maximum displacement under the

TABLE 1. Properties of PLA composites.

Fiber content /%	Density /g/cm^3	Tensile strength /MPa	Tensile modulus /MPa	Poisson's ratio
0	1.25	72.0	1384.6	0.23
10	1.375	89.1	2209.58	0.22
20	1.5	109.6	2878.76	0.21
30	1.625	124.3	3742.9	0.21
40	1.75	138.2	4362.52	0.20
50	1.875	140.8	5005.88	0.20
60	2	136.1	4350.54	0.19

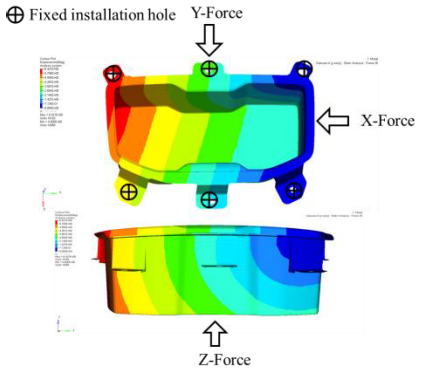

FIGURE 4. Loading position and loading direction.

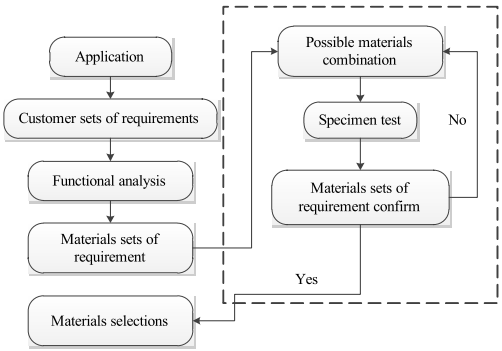

FIGURE 5. Multi-material design process.

three-direction force respectively and the modal of the original product with OptiStruct. Material in the analysis is Polypropylene (PP) with the elastic modulus of 2739 MPa and the density of 1.21g/cm^3. Figure 4 illustrates the 3D model and prescribed boundary conditions which all DOFs are fixed. Loading position of three-direction force are set at center of each surface.

IV. OPTIMIZATION DESIGN

A. MULTI-MATERIAL OPTIMAL DESIGN METHOD

A light-weight structure exhibiting good performance can be realized via the multi-materials optimal design method performed with multi-material additive manufacturing (MMAM) technology. This method allows objective material selection for a given application, and the reflex of choosing the typically employed materials is avoided. In turn, structures can be simplified, complicated assemblies removed, and performance improved, while avoiding many of the difficulties associated with material selection [47]. A multi-material design process can be described as follows:

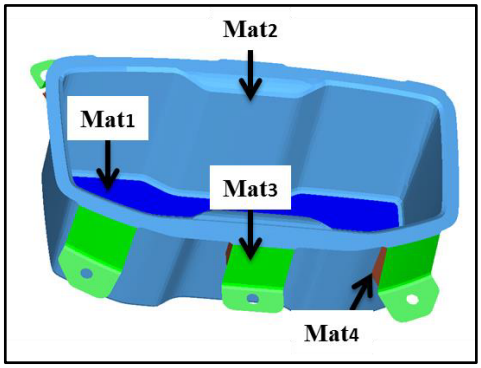

FIGURE 6. Disassembly of product.

According to the original part, the thickness of Mat1, Mat2, Mat3 and Mat4 are 2.8mm, 2mm, 1.2mm and 1.8mm respectively. For full-capacity operation of the PLA composites, the PLA part is separated into four components that can be fabricated as PLA composites (see Figure 6) with different basalt fiber (BF) content. With multi-material 3D printing technology, four components are integrated one component. The multi-material design is based on the customer requirements for the final product. During the functional analysis, the customer requirements are translated into technical terms. The interior trim part should have a certain stiffness and avoid the resonance effect. Customer requirements of this case are translated in the stiffness and the first-order modal of the original part.

B. OPTIMIZATION STRATEGY AND OPTIMIZATION ALGORITHM

Many material combinations satisfy the requirements. An ideal design is required for finding the minimum mass

corresponding to the objective of the product. The optimization objective of the product can be expressed as follows:

$$\begin{aligned} &\min\ f(x_i) \\ &s.t.\ g_1(x_i) \le \text{value1} \\ &\quad g_2(x_i) \le \text{value2} \\ &\quad g_3(x_i) \le \text{value3} \\ &\quad g_4(x_i) \ge \text{value4} \quad i = 1, 2, 3, 4 \end{aligned} \tag{1}$$

X_i (i = 1, 2, 3, 4): BF content of the four components, $f(x_i)$: mass of the PLA product, $g_1(x_i)$, $g_2(x_i)$, and $g_3(x_i)$: X-, Y-, and Z-direction maximum displacements, respectively, and $g_4(x_i)$: frequency of the first-order modal. Value1, value2, value3: X-, Y-, and Z-direction maximum displacements, respectively, and value4: first-order modal of original product. Value1, value2, value3 and value4 are set as constraints in the optimal process.

In this work, a mathematical model of the optimum design for the material parameters based on the minimum mass is used to search for the best combination. During the optimization procedure, MIGA is used to find the global optimum in a given design space.

MIGA is based on a Traditional Genetic Algorithm (TGA), where the population is divided into several islands. Traditional genetic operations are separately performed on each island, and individuals then undergo inter-island migration. Furthermore, MIGA searches many designs and multiple locations of the design space. The main feature distinguishing MIGA from the traditional genetic algorithms is the fact that each population of individuals is divided into several subpopulations referred to as 'islands'. The selection operation in MIGA employs the so-called 'tournament selection' scheme. In this process, the best individuals are selected from a small subset of randomly selected individuals (rather than from the entire population). This scheme allows for duplicate individuals in the child population.

The performance of the algorithm depends on the parameters. For example, the migration process is determined by the migration interval (i.e., the number of generations between each migration) and the migration rate (i.e., the percentage of individuals migrating from each island). Through MIGA, a local optimal solution and premature convergence can be avoided. The parameters of MIGA are listed in Table 2.

C. KRIGING SURROGATE MODEL

Analysis of the sampling results constitutes the main activity in the search for a Pareto-optimal Solution. In this work, the computational time is minimized by using the Kriging surrogate model as an approximation. The Kriging approximation model represents one type of unbiased estimation model that is characterized by minimum variance. This model is capable of local estimation and provides good fitting for complex (i.e., highly non-linear) problems. Moreover, the model uses a sum of a constant and a random process to represent the response values of the system and is composed of regression polynomials and a stochastic term. The surrogate model can

TABLE 2. Detailed parameters of MIGA.

Parameters of setup	Value
Sub-population size	10
Number of islands	10
Number of generations	10
Rate of crossover	1.0
Rate of migration	0.01
Interval of migrations	5
Penalty multiplier	1000
Penalty exponent	2
Maximum failed runs	5

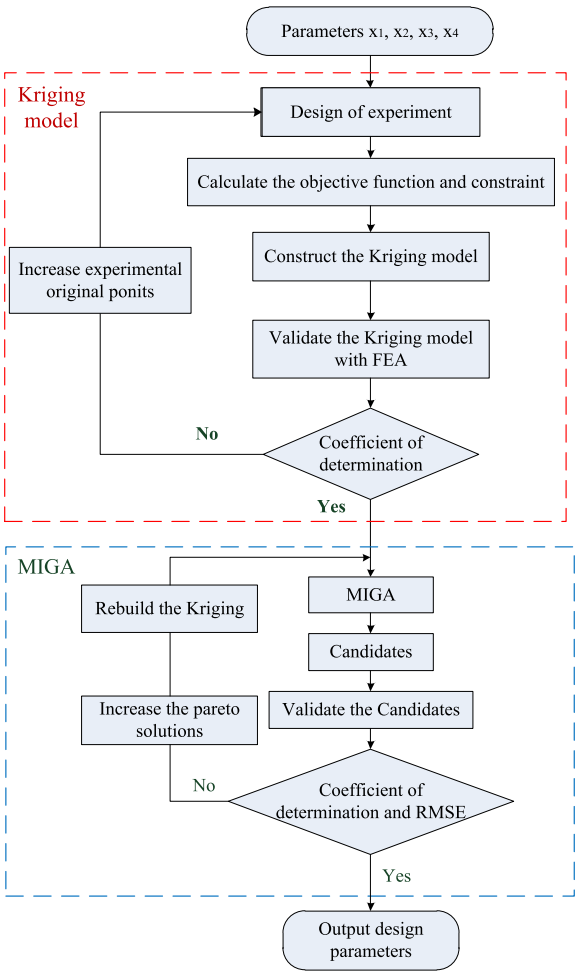

FIGURE 7. Implementation procedure.

be described by the following expressions:

$$y(x) = f(x^T)\beta + Z(x) \tag{2}$$

$f(x) = [f_1(x)f_2(x)\cdots f_q(x)]^T$ is the regression polynomial and $\beta = [\beta_1\beta_2\cdots\beta_q]^T$ is the regression coefficient. $Z(x)$ is a stochastic term with a mean value of zero. The Kriging surrogate model is established using original points and responses.

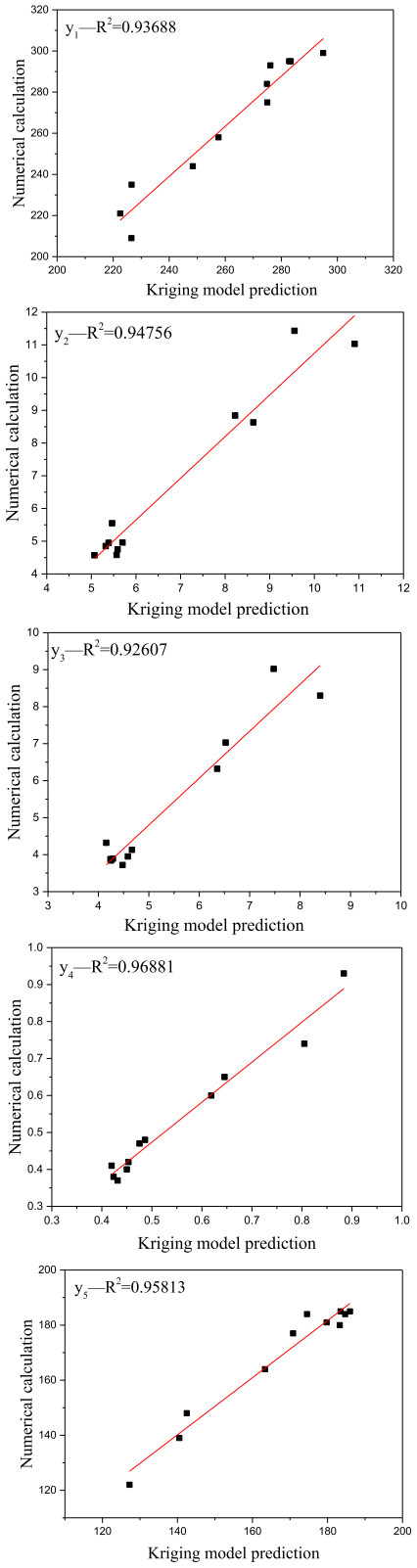

FIGURE 8. Error analysis of the R^2 associated with five responses.

The design parameters in this study (i.e., x_1, x_2, x_3, and x_4, see Figure 6) represent the BF fiber content of Mat1, Mat2, Mat3, and Mat4, respectively. In addition, the objective function $f(x_i)$ denotes the mass of the product and $g(x_i)$ is the constraint. The optimization process is implemented by combining the Kriging model with MIGA, as shown in Figure 7. This process consists of the following steps:

a) Original points are generated by using the Optimal Latin hypercube experiment design for the surrogate model.
b) The Kriging model is used to determine the relationships between the design parameters and the responses that comprise the objective function and constraint. The effectiveness is evaluated in terms of R^2.
c) The validity of the model is confirmed using sample points (except for original points).
d) MIGA is used to determine the optimal geometries, and the accuracy of the process is verified.

V. RESULTS AND DISCUSSION

A. SURROGATE-MODEL IMPROVEMENT

The optimal Latin delta hypercube design enables even distribution of all the test points as well as very good spatial filling and equalization in the design space. Compared with orthogonal experiments, optimal Latin hypercube designs allow the investigation of more combinations with the same number of points. The original sample points generated by the hypercube design are listed in a table. After the response model is constructed, the error analysis method based on the coefficient of determination (R^2) is used to assess the prediction accuracy of the surrogate model. Three sets of sample points are selected for verifying the effectiveness of the model (see Table 3).

The results in the table show that the prediction of the original points by the Kriging model is the same as the response of the original points. The R^2 values indicate that the model provides an unbiased estimate of the original points. Nevertheless, the prediction of the other three points yields the opposite result. The R^2 values are all <0.9, indicating that the precision of the model falls short of the required levels. This low precision results from (among others) an inadequate coverage ratio of the original points. The Kriging model ensures the accuracy of the figures near the original points. However, the values of the three points used to verify the model deviate from the original points and, hence, the number of original points must be increased.

The influence of Poisson's ratio is small and is therefore ignored. According to previous studies and finite element theory, the tensile modulus plays a key role in the simulation of elastic deformation. Therefore, in this work, we focus exclusively on this parameter. The functional relationship between the tensile modulus and the BF content is established through a non-linear regression equation and the values of the PLA composites with differing BF content (the content is 0, 1, 2, 3, $\cdots$, 60) are determined from:

$$j(x) = a_1 + a_2 \cdot x + a_3 \cdot x^2 \cdots a_{n+1}x^n \tag{3}$$

$j(x)$ is the tensile modulus and $a_1, a_2, \ldots, a_{n+1}$ are the polynomial coefficients. Using the least-squares method,

TABLE 3. Original sample points.

No	X_1	X_2	X_3	X_4	$f(x_i)$	$g_1(x_i)$	$g_2(x_i)$	$g_3(x_i)$	$g_4(x_i)$
1	10	40	60	20	263	5.08	4.192	0.67	178
2	20	0	30	0	208	12.62	10.45	0.77	121
3	60	20	50	30	254	6.64	5.39	0.47	157
4	40	60	40	60	301	5.07	4.06	0.42	130
5	50	10	0	40	227	11.51	8.25	0.51	147
6	30	50	10	10	276	5.76	4.48	0.46	190
7	0	30	20	50	242	6.32	4.9	0.99	172
R^2					1	1	1	1	1
Kriging-1	6	39	24	58	252	7.51	5.92	0.61	156
Kriging-2	36	56	36	52	257	7.32	5.74	0.59	154
Kriging-3	59	53	31	37	253	7.51	5.93	0.60	156
FEA-1	6	39	24	58	258	5.55	4.32	0.74	181
FEA-2	36	56	36	52	293	4.85	3.84	0.42	180
FEA-3	59	53	31	37	295	4.95	3.89	0.41	185
R^2					0.52	0.39	0.47	0.11	0.29

TABLE 4. Original points of improvement model.

	No	X_1	X_2	X_3	X_4	$f(x_i)$	$g_1(x_i)$	$g_2(x_i)$	$g_3(x_i)$	$g_4(x_i)$
Original points	1	35	17	37	39	239	7.28	5.8	0.51	155
	2	28	10	55	54	231	8.17	6.47	0.59	142
	3	16	42	48	53	260	4.7	3.8	0.58	183
	4	56	41	25	59	277	5.39	4.19	0.4	184
	5	42	26	60	35	258	6.18	4.96	0.44	164
	6	51	15	26	56	240	8.02	6.25	0.46	153
	7	57	16	9	14	238	8.95	7.02	0.49	156
	8	15	24	51	0	243	6.23	5.34	0.65	162
	9	48	3	18	34	220	11.5	8.89	0.53	133
	10	29	47	13	4	272	5.72	4.55	0.48	187
	⋮	⋮	⋮	⋮	⋮	⋮	⋮	⋮	⋮	⋮
	50	6	39	24	58	272	5.69	4.58	0.4	185
Test points	51	36	56	36	52	258	5.55	4.32	0.74	181
	52	59	53	31	37	293	4.85	3.84	0.42	180
	⋮	⋮	⋮	⋮	⋮	⋮	⋮	⋮	⋮	⋮
	61	10	48	52	7	275	4.57	3.88	0.65	185

the original points for fitting the functional relationship are determined from

$$j(x) = 13.79179 + 1.10368 \cdot x - 0.03735 \cdot x^2 + 0.00127 \cdot x^3 - 0.000013652 \cdot x^4 \quad (4)$$

The accuracy (i.e., effectiveness of the model) is described relative to R^2 and RMSE values of 0.99322 and 0.5246, respectively. The tensile modulus is expressed in terms of equation (4), and the 61 original points generated for the Kriging model are listed in a table (see Table 4). These points are generated through an optimal Latin hypercube experiment design, and responses are calculated via numerical simulation. Eleven of the original sample points are used to check the accuracy of the model.

TABLE 5. RSM coefficients and R^2.

Polynomial	Coefficients				
	$f(x_i)$	$g_1(x_i)$	$g_2(x_i)$	$g_3(x_i)$	$g_4(x_i)$
Constant	183.6582653	13.75703975	10.97306219	1.12493528	125.5025935
x_1	0.732835222	0.015863708	0.008939466	-0.021875123	-0.081438775
x_2	1.54030186	-0.283945851	-0.227361262	-0.008504884	2.434284649
x_3	0.351491233	-0.101863638	-0.059563023	-0.001589101	-0.02907511
x_4	0.324949683	-0.006304663	-0.024776872	0.000957594	-0.069525615
x_1^2	-0.003293687	-0.000189177	-0.000136731	0.000217847	0.001180648
$x_1 \cdot x_2$	-0.000943237	-2.84E-05	-9.44E-06	3.27E-05	-0.001038921
$x_1 \cdot x_3$	-0.005848311	-5.50E-05	4.62E-06	1.11E-05	0.00152219
$x_1 \cdot x_4$	-0.002848094	3.26E-05	4.00E-05	-1.44E-05	0.001399807
x_2^2	-0.001080289	0.002737228	0.002146249	7.11E-05	-0.024980366
$x_2 \cdot x_3$	-0.001692836	0.000406794	0.000350724	7.55E-06	-0.00060401
$x_2 \cdot x_4$	-0.002598324	0.000223116	0.000267474	-2.71E-06	0.002253265
x_3^2	0.002114212	0.00081422	0.000373042	9.11E-06	-0.00155802
$x_3 \cdot x_4$	-0.003729292	0.00012714	0.000160502	9.92E-07	0.000623321
x_4^2	-0.000625689	-0.000128124	3.88E-05	-7.73E-06	-0.000580244
R^2	0.97669	0.98601	0.98327	0.98984	0.97638

The effectiveness of the model is determined with test points. The Kriging model provides quite precise predictions of the responses associated with the original points and, hence, R^2 is always one. The test points are used to confirm this precision by comparing the predicted responses with those of the numerical simulations. As previously reported in several studies, the response model exhibits good predictive capability, as evidenced by R^2 values larger than 0.9 [48]. As shown in Figure 8, for the design conditions considered, the R^2 of each response is >0.92. This confirms the predictive capability of the Kriging model and, in turn, its applicability to the results obtained in this work.

A response surface model is built for comparison with the Kriging model. The response surface has been used successfully in establishing the non-linear input-output relationships, which are required for the predictive capabilities of the model. The RSM, is based on a set of mathematical and statistical techniques. This model uses multiple regression equations to express the complex implicit relationship between the objective and the design variables. The model can be accurately built with experimental points, and continuity as well as controllability of the design variables are required. Generally, a second-order model is used to construct the RSM. For the case of n variables, the two-order polynomial response surface model is described by

$$y(x) = \beta_0 + \sum_{i=1}^{n} \beta_i x_i + \sum_{i}^{n} \beta_{ii} x_i^2 + \sum_{i=2}^{n} \sum_{j=1}^{i=1} \beta_{ij} x_i x_j \quad (5)$$

x denotes the design variables and β is the coefficient.

Unlike the Kriging model, five RSMs are needed for each response. A genetic algorithm (rather than a least squares method typically used in other studies) is used to fit the coefficient. The fitness threshold is set as the difference between the predicted value and the actual value (the corresponding RSM coefficients are listed in Table 5). The R^2 values are all >0.97 suggesting that, compared with the Kriging model, the quadratic regression (function) of GA-based RSM has the same ability to predict the results.

B. OPTIMIZATION OF THE CONFIGURATION AND RESULTS

Using an effective surrogate model, the optimization process can be effectively executed with the constraints. The result computed in the form page is shown in a table (see Table 6), and the values are set as boundary conditions for optimization.

The mass objective function and the mathematical optimization model are governed by the following conditions

$$\begin{aligned} &\min f(x_i) \\ &s.t.\ g_1(x_i) \le 9.6 \\ &\quad g_2(x_i) \le 7.8 \\ &\quad g_3(x_i) \le 0.7 \\ &\quad g_4(x_i) \ge 160 \quad i = 1, 2, 3, 4 \end{aligned} \quad (6)$$

Based on the optimization strategy, two surrogate models are used in the process. The Kriging and RSM models converge at 971 and 986 results, respectively. A plot of the mass history (see Figure 9) indicates that the mass of the part fluctuates significantly in the initial stages and

TABLE 6. Constraints of the optimal process.

	X-displacement/mm	Y-displacement/mm	Z-displacement/mm	Modal/Hz
Value	9.633	7.876	0.708	160
Boundary conditions for PLA product	$\leqslant$	$\leqslant$	$\leqslant$	$\geqslant$

TABLE 7. Results and error analysis.

	x_1	x_2	x_3	x_4	$f(x_i)$	$g_1(x_i)$	$g_2(x_i)$	$g_3(x_i)$	$g_4(x_i)$
Kriging	16.5	21.6	14.1	10.2	231.8	8.5	6.6	0.68	162.5
N-S	16	21	14	10	232.6	7.9	6.4	0.68	161
Residuals	—	—	—	—	0.003	0.073	-0.030	0.000	-0.009
RSM	22.1	19.9	0.02	10.6	230.3	9.4	7.2	0.63	162.5
N-S	22	20	1	11	230.4	8.8	7.4	0.64	160.2
Residuals	—	—	—	—	0.001	0.061	0.025	0.021	0.014
Constraints	—	—	—	—	—	9.6	7.8	0.7	160
One material					253.7	7.5	6.9	0.58	172

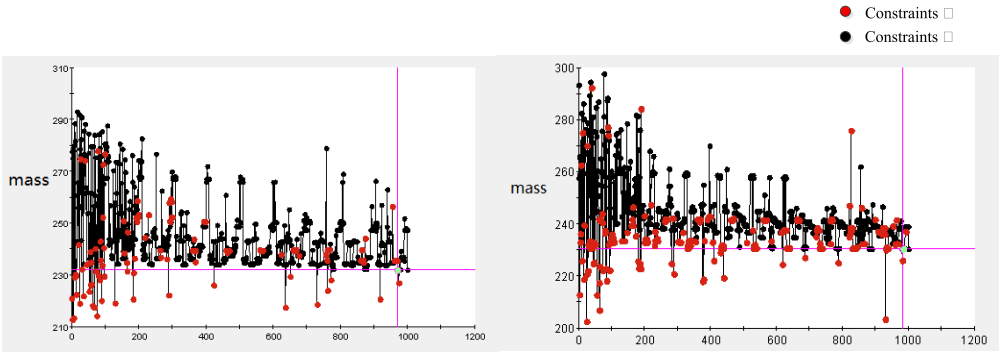

Kriging model RSM model

FIGURE 9. History of MIGA searching.

approaches the optimum value as the number of evolutions increase. Optimization of the minimum mass yields feasibility of the final design and prevents instability. The Kriging model results, RSM results, constraints, and material design results are shown in Table 9. To validate the optimization results, a rounding method is applied to the parameters of the numerical simulation (N-S). The accuracy of the results is represented by residuals. Except for the residuals associated with the $g_1(x_i)$, the residuals of the Kriging and RSM models are all lower than the specified limits (generally, residuals lower than 5% meet the requirements). This is attributed to the rounding procedure. However, the values of $g_1(x_i)$ lie within the constraints and are, therefore, acceptable. Furthermore, the mass of the PLA composite product decreases (by ∼9%) from 253.7 to 232.6 g and 230.4 g (Table 7), indicating that product-design optimization aimed at achieving light-weight products can be realized via MIGA.

C. CORRELATION ANALYSIS

The correlation analysis is based on the Pearson and Spearman correlation, which is a linear analysis method. As in sensitivity analysis, with this method, the mode of the important parameters can be included in the objective function. The value of the correlation coefficient (denoted as r) indicates the correlation between the model parameters and the responses. The r_{xy} r values can be obtained as follows:

$$r_{xy} = \frac{\sum (X-\overline{X})(Y-\overline{Y})}{\sqrt{\sum (X-\overline{X})^2}\sqrt{(Y-\overline{Y})^2}} = \frac{\sum xy}{\sqrt{\sum x^2}\sqrt{\sum y^2}} = \frac{S_{XY}}{S_X S_Y} \tag{7}$$

$$S_{XY} = \frac{\sum (X-\overline{X})(Y-\overline{Y})}{n-1} \tag{8}$$

$$S_X = \sqrt{\frac{\sum (X-\overline{X})^2}{n-1}} \tag{9}$$

$$S_Y = \sqrt{\frac{\sum (Y-\overline{Y})^2}{n-1}} \tag{10}$$

The positive value of r corresponds to an increase in the response with increasing number of input parameters, until a value of one (i.e., the limit of r) is reached.

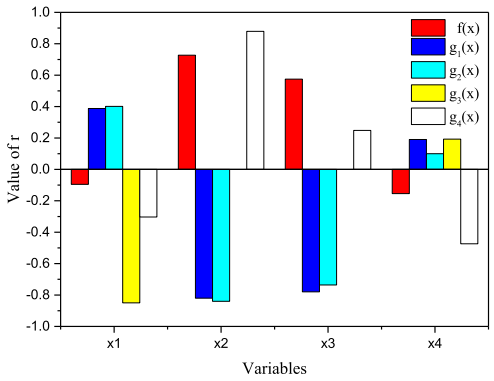

FIGURE 10. Correlation coefficient of parameters.

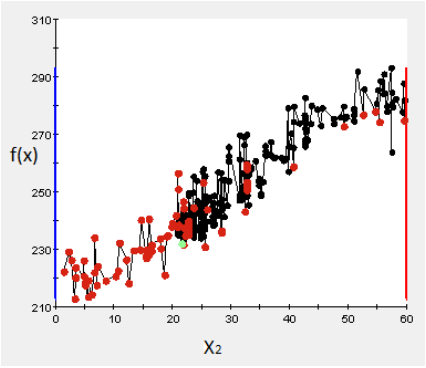

FIGURE 11. Effect of x_2 on the f(x).

Negative values have the opposite effect on the objective function. The results of the correlation analysis are shown in Figure 10. As the figure shows, the parameters x_2 and x_3 (with values of 0.72 and 0.57, respectively) have a positive effect on the objective function, indicating that the mass increases with increasing x_2 and x_3. Compared with x_3, x_2 has a stronger impact on the mass, suggesting that the mass may be most effectively reduced by reducing the value of x_2.

VI. CONCLUSIONS

In this study, an internal part of an automotive is designed with environmentally friendly PLA composites. The mechanical properties of these BF-reinforced PLA composites are obtained via standard tests. The product design constraints are analyzed and set through actual load testing. For effective use of the materials, the original part is divided (via the multi-materials optimal design method) into four components with different materials. A MIGA-based optimization design approach is proposed for finding the optimal solution using Kriging and RSM surrogate models. The conclusions of this study are as follows:

1) The main mechanical properties of BF-reinforced PLA approach those of PP used in the original product. More importantly, BF-reinforced PLA constitutes a suitable green material for replacing the petroleum-based materials considered in this case.
2) The Kriging surrogate model is used to determine the non-linear relationship. The RSM surrogate model is compared with the Kriging surrogate model. Values of $R^2 > 0.92$ indicate that good accuracy is obtained by improving the performance prediction of the original points. Correlation analysis shows that material 2 has the strongest impact on the mass.
3) Using the above algorithms, the mass of the PLA composite product is reduced (by ∼9%) from 253.7 to 232.6 g and 230.4 g, indicating that product-design optimization is possible via the proposed process. Correlation analysis shows that material 2 has the strongest impact on the mass.
4) The optimization process proposed for the multi-material optimal design is feasible and contributes significantly to the attainment of light-weight vehicle parts. The results of the improvement indicate the universality and effectiveness of this approach.

Further, fatigue properties of PLA materials will be researched and the reliability of the component will be considered in future component design with PLA composites as the reliability of component is also a vital property for automotive part design.

ACKNOWLEGMENT

The authors would like to thank the Key Laboratory of Polymer Ecomaterials (Changchun Institute of Applied Chemistry, Chinese Academy of Sciences, Changchun) for allowing the use of their laboratory.

REFERENCES

[1] N. Wu and H. Zhang, "Mechanical properties and phase morphology of super-tough PLA/PBAT/EMA-GMA multicomponent blends," *Mater. Lett.*, vol. 192, pp. 17–20, Apr. 2017.
[2] G. Tian, M. Zhou, and P. Li, "Disassembly sequence planning considering fuzzy component quality and varying operational cost," *IEEE Trans. Autom. Sci. Eng.*, vol. 15, no. 2, pp. 748–760, Apr. 2018.
[3] E. Castro-Aguirre, F. Iñiguez-Franco, H. Samsudin, X. Fang, and R. Auras, "Poly(lactic acid)—Mass production, processing, industrial applications, and end of life," *Adv. Drug Del. Rev.*, vol. 107, pp. 333–366, Dec. 2016.
[4] S. Farah, D. G. Anderson, and R. Langer, "Physical and mechanical properties of PLA, and their functions in widespread applications—A comprehensive review," *Adv. Drug Del. Rev.*, vol. 107, pp. 367–392, Dec. 2016.
[5] C. S. Boland, R. De Kleine, G. A. Keoleian, E. C. Lee, H. C. Kim, and T. J. Wallington, "Life cycle impacts of natural fiber composites for automotive applications: Effects of renewable energy content and lightweighting," *J. Ind. Ecol.*, vol. 20, no. 1, pp. 179–189, 2016.
[6] S. K. Jeoung *et al.*, "Aerobic biodegradability of polyester/polylactic acid composites for automotive NVH parts," *Int. J. Precis. Eng. Manuf.*, vol. 15, no. 8, pp. 1703–1707, 2014.
[7] A. Bouzouita *et al.*, "Design of highly tough poly(L-lactide)-based ternary blends for automotive applications," *J. Appl. Polym. Sci.*, vol. 133, no. 19, 2016.
[8] Y. Guo, L. Wang, D. Cheng, J. Shao, and H. Hou, "Toughening behavior of poly(L-lactic acid)/poly(D-lactic acid) asymmetric blends," *Polym.-Plastics Technol. Eng.*, vol. 57, no. 12, pp. 1225–1235, 2018.
[9] A. Rahim *et al.*, "Vehicular social networks: A survey," *Pervasive Mobile Comput.*, vol. 43, pp. 96–113, Jan. 2018.
[10] X. Sun, H. Zhang, T. Peng, K. Li, R. Zhang, and W. Meng, "Primary resonance analysis and vibration suppression for the harmonically excited nonlinear suspension system using a pair of symmetric viscoelastic buffers," *Nonlinear Dyn.*, Jun. 2018, doi: 10.1007/s11071-018-4421-9.

[11] X. J. Kong *et al.*, "Mobility dataset generation for vehicular social networks based on floating car data," *IEEE Trans. Veh. Technol.*, vol. 67, no. 5, pp. 3874–3886, May 2018.

[12] G. D. Tian *et al.*, "Operation patterns analysis of automotive components remanufacturing industry development in China," *J. Cleaner Prod.*, vol. 164, pp. 1363–1375, Oct. 2017.

[13] G. Koronis, A. Silva, and M. Fontul, "Green composites: A review of adequate materials for automotive applications," *Compos. B, Eng.*, vol. 44, no. 1, pp. 120–127, 2013.

[14] S. K. Ramamoorthy, M. Skrifvars, and A. Persson, "A review of natural fibers used in biocomposites: Plant, animal and regenerated cellulose fibers," *Polym. Rev.*, vol. 55, no. 1, pp. 107–162, Jan. 2015.

[15] R.-H. Zhang, Z.-C. He, H.-W. Wang, F. You, and K.-N. Li, "Study on self-tuning tyre friction control for developing main-servo loop integrated chassis control system," *IEEE Access*, vol. 5, pp. 6649–6660, 2017.

[16] Z. Ying, D. Wu, M. Zhang, and Y. Qiu, "Polylactide/basalt fiber composites with tailorable mechanical properties: Effect of surface treatment of fibers and annealing," *Compos. Struct.*, vol. 176, pp. 1020–1027, Sep. 2017.

[17] T. TÃąbi, P. Bakonyi, S. Hajba, P. J. Herrera-Franco, T. Czigány, and J. G. Kovács, "Creep behaviour of injection-moulded basalt fibre reinforced poly(lactic acid) composites," *J. Reinforced Plastics Compos.*, vol. 35, no. 21, pp. 1600–1610, 2016.

[18] A. A. J. Kumar and V. Srinivasan, "Thermal characteristics of chitosan dispersed poly lactic acid/basalt hybrid composites," *Mater. Express*, vol. 6, no. 4, pp. 337–343, Aug. 2016.

[19] A. Zegaoui *et al.*, "High-performance polymeric materials with greatly improved mechanical and thermal properties from cyanate ester/benzoxazine resin reinforced by silane-treated basalt fibers," *J. Appl. Polym. Sci.*, vol. 135, no. 21, p. 46283, Jun. 2018.

[20] A. H. Sakhaei, S. Kaijima, T. L. Lee, Y. Y. Tan, and M. L. Dunn, "Design and investigation of a multi-material compliant ratchet-like mechanism," *Mechanism Mach. Theory*, vol. 121, pp. 184–197, Mar. 2018.

[21] F. Xiong, D. Wang, Z. Ma, S. Chen, T. Lv, and F. Lu, "Structure-material integrated multi-objective lightweight design of the front end structure of automobile body," *Struct. Multidisciplinary Optim.*, vol. 57, no. 2, pp. 829–847, Feb. 2018.

[22] H. Xiong, X. Zhu, and R. Zhang, "Energy recovery strategy numerical simulation for dual axle drive pure electric vehicle based on motor loss model and big data calculation," *Complexity*, vol. 2018, Aug. 2018, Art. no. 4071743, doi: 10.1155/2018/4071743.

[23] A. I. Taub and S. S. Babu, "Opportunities and challenges for introducing new lightweight metals in transportation," *Int. J. Powder Metall.*, vol. 54, no. 2, pp. 27–33, Apr. 2018.

[24] G. Tian, H. Zhang, M. Zhou, and Z. Li, "AHP, gray correlation, and TOPSIS combined approach to green performance evaluation of design alternatives," *IEEE Trans. Syst., Man, Cybern., Syst.*, vol. 48, no. 7, pp. 1093–1105, Jul. 2018.

[25] S. Stoycheva, D. Marchese, C. Paul, S. Padoan, A.-S. Juhmani, and I. Linkov, "Multi-criteria decision analysis framework for sustainable manufacturing in automotive industry," *J. Cleaner Prod.*, vol. 187, pp. 257–272, Jun. 2018.

[26] S. S. Yang, N. Nasr, S. K. Ong, and A. Y. C. Nee, "Designing automotive products for remanufacturing from material selection perspective," *J. Cleaner Prod.*, vol. 153, no. 1, pp. 570–579, Jun. 2017.

[27] A. Bandyopadhyay and B. Heer, "Additive manufacturing of multi-material structures," *Mater. Sci. Eng. R, Rep.*, vol. 129, pp. 1–16, Jul. 2018.

[28] M. Morreale, M. C. Mistretta, and V. Fiore, "Creep behavior of poly(lactic acid) based biocomposites," *Materials*, vol. 10, no. 4, p. 395, Apr. 2017.

[29] F. S. Senatov, K. V. Niaza, A. A. Stepashkin, and S. D. Kaloshkin, "Low-cycle fatigue behavior of 3d-printed PLA-based porous scaffolds," *Compos. B, Eng.*, vol. 97, pp. 193–200, Jul. 2016.

[30] Y. Pu, F. Ma, J. Zhang, and M. Yang, "Optimal lightweight material selection for automobile applications considering multi-perspective indices," *IEEE Access*, vol. 6, pp. 8591–8598, 2018.

[31] X. Hu, X. Chen, Y. Zhao, and W. Yao, "Optimization design of satellite separation systems based on multi-island genetic algorithm," *Adv. Space Res.*, vol. 53, no. 5, pp. 870–876, 2014.

[32] B. Song, D. Lyu, and J. Jiang, "Optimization of composite ring stiffened cylindrical hulls for unmanned underwater vehicles using multi-island genetic algorithm," *J. Reinforced Plastics Compos.*, vol. 37, no. 10, pp. 668–684, Mar. 2018.

[33] C. Han, L. Wang, Z. Zhang, J. Xie, and Z. Xing, "A multi-objective genetic algorithm based on fitting and interpolation," *IEEE Access*, vol. 6, pp. 22920–22929, 2018.

[34] X. Kong, X. Song, F. Xia, H. Guo, J. Wang, and A. Tolba, "LoTAD: Long-term traffic anomaly detection based on crowdsourced bus trajectory data," *World Wide Web*, vol. 21, no. 3, pp. 825–847, 2018.

[35] Z. Wang, J. Ma, and L. Zhang, "State-of-health estimation for lithium-ion batteries based on the multi-island genetic algorithm and the Gaussian process regression," *IEEE Access*, vol. 5, pp. 21286–21295, 2017.

[36] Y. Zhang, S. Hu, Y. Zhang, and L. Chen, "Optimization and analysis of centrifugal pump considering fluid-structure interaction," *Sci. World J.*, vol. 2014, Aug. 2014, Art. no. 131802.

[37] D.-H. He, D.-S. Li, X.-Q. Li, and C.-H. Jin, "Optimization on springback reduction in cold stretch forming of titanium-alloy aircraft skin," *Trans. Nonferrous Met. Soc. China*, vol. 20, no. 12, pp. 2350–2357, Dec. 2010.

[38] N. Jansson, W. D. Wakeman, and J.-A. E. Månson, "Optimization of hybrid thermoplastic composite structures using surrogate models and genetic algorithms," *Compos. Struct.*, vol. 80, no. 1, pp. 21–31, Sep. 2007.

[39] W. Hao, Y. Ying, Y. Wei, and L. Baohua, "Adaptive approximation-based optimization of composite advanced grid-stiffened cylinder," *Chin. J. Aeronaut.*, vol. 23, no. 4, pp. 423–429, Aug. 2010.

[40] H.-S. Jeong and K.-Y. Kim, "Shape optimization of a feedback-channel fluidic oscillator," *Eng. Appl. Comput. Fluid Mech.*, vol. 12, no. 1, pp. 169–181, Oct. 2017.

[41] Z. Zhang, J. Song, Y. Liu, and D. Xu, "An integrated multidisciplinary design optimization method for computer numerical control machine tool development," *Adv. Mech. Eng.*, vol. 7, no. 2, Feb. 2015.

[42] J.-C. Yu and Suprayitno, "Evolutionary reliable regional Kriging surrogate and soft outer array for robust engineering optimization," *IEEE Access*, vol. 5, pp. 16520–16531, 2017.

[43] R. Paz, E. Pei, M. Monzón, F. Ortega, and L. Suárez, "Lightweight parametric design optimization for 4D printed parts," *Integr. Comput.-Aided Eng.*, vol. 24, no. 3, pp. 225–240, 2017.

[44] Y. Yang, W. Zeng, W.-S. Qiu, and T. Wang, "Optimization of the suspension parameters of a rail vehicle based on a virtual prototype Kriging surrogate model," *Proc. Inst. Mech. Eng. F, J. Rail Rapid Transit*, vol. 230, no. 8, pp. 1890–1898, Nov. 2016.

[45] M. Li, G. Li, and S. Azarm, "A Kriging metamodel assisted multi-objective genetic algorithm for design optimization," *J. Mech. Des.*, vol. 130, no. 3, p. 031401, 2008.

[46] H.-Y. Tang, H.-Y. Ye, X.-P. Chen, C. Qian, X.-J. Fan, and G.-Q. Zhang, "Numerical thermal analysis and optimization of multi-chip LED module using response surface methodology and genetic algorithm," *IEEE Access*, vol. 5, pp. 16459–16468, 2017.

[47] F. X. Kromm, J. M. Quenisset, T. Lorriot, R. Harry, and H. Wargnier, "Definition of a multimaterials design method," *Mater. Des.*, vol. 28, no. 10, pp. 2641–2646, 2007.

[48] W. Wang, S. Yuan, J. Pei, and J. Zhang, "Optimization of the diffuser in a centrifugal pump by combining response surface method with multi-island genetic algorithm," *Proc. Inst. Mech. Eng., E, J. Process Mech. Eng.*, vol. 231, no. 2, pp. 191–201, 2016.

FANGWU MA received the B.S. and M.S. degrees in automotive engineering from Jilin University (former Jilin University of Technology), Changchun, China, in 1982 and 1988, respectively, and the Ph.D. degree in mechanical engineering from the Imperial College London, London, U.K., in 1999. Then, he worked as a Research Fellow on transportation design at the University of Wolverhampton, U.K., in 1990.

He was a Senior Engineer at Chrysler LLC, taking charge of the Vehicle Research and development programs including Jeep Liberty, Dodge Ram, and Caravan. Then, he was the Chief Engineer and the Vice President of the Geely R&D Centre, in charge of developing GC7, GX7, and GX9, as well as the negotiation and recruitment training of IP and DDR during Geely Auto's Acquisition of Volvo. He is the Executive Dean of the Qingdao Automotive Research Institute, Jilin University. He is a SAE-China Fellow. He is the National "Thousand Talents Plan" Distinguished Experts. He also serves as the Executive Editor-in-Chief of the Automotive Innovation–the English Edition of automotive engineering.

He has published numerous technical papers, reviewed technical papers for SAE and other journals to enhance quality of publication, and invented patents related to automotive engineering. Furthermore, he has actively participated, organized, and contributed to many automotive related conference worldwide, such as SAE World Congress, Automotive Design Conference in Interior Motive, International Forum on Chinese Automobile Recycling, FISITA World Automotive Congress & Exhibition, International Conference on Globalization of Development and Innovation, International AVL Conference on Engine & Environment, JSAE Annual Spring Congress, and International Conference on NVH Technology.

LU HAN received the B.E. degrees in industrial design engineering (Autobody) from Jilin University, Changchun, China, in 2010, and the M.S. degrees in body engineering from Jilin University, Changchun, in 2013, where he is currently pursuing the Ph.D. degree in vehicle engineering with the College of Automotive Engineering. He was with the Autobody Research Department for FEA, RDC, FAW, for two years. Then, he was with the Vehicle Reliability Study Department for load analysis for two years. His research interests include automotive bio-based materials and lightweight design.

YANG ZHOU received the B.S. degree in automotive engineering from Jilin University, Changchun, China, in 2010. Then, he was the Chief Engineer at the FAW R&D Centre, where he was in charge of the EXT of developing JiaBaoV80 V60, Senya R7. He is currently a Chief Engineer at FAW Car Co., Ltd. His work focus are auto interior ornaments and automotive lightweight.

SHIXIAN CHEN received the B.S. degree in mechanical design manufacture and automation major from Dezhou University, Dezhou, China, in 2014, and the M.A. degree in mechanical manufacture and automation major from the Changchun University of Science and Technology, Changchun, China, in 2017. He is currently pursuing the Ph.D. degree in vehicle engineering with the College of Automotive Engineering, Jilin University. His research interests include automotive lightweight materials, composite materials and polymer-metal hybrid. He has five papers published which are indexed by SCI or EI.

YONGFENG PU received the B.S. and M.S. degrees in agricultural mechanization and automation from Jilin University, Changchun, China, in 2008 and 2015, respectively. He is currently an Assistant Researcher and also the Ph.D. candidate of automotive body engineering at the College of Automotive Engineering, Jilin University. His research focus are automotive lightweight materials and composite materials. He has published a paper in IEEE Access.